

# A Tool for 3D Representation of the 2D Thermographic Breast Acquisitions

Eudoxia L. S. Moura<sup>1,3</sup><sup>a</sup>, Gleidson M. Costa<sup>2</sup><sup>b</sup>, Tiago B. Borchardt<sup>2</sup><sup>c</sup> and Aura Conci<sup>3</sup><sup>d</sup>

<sup>1</sup>Federal Institute of Education, Science and Technology of Rondônia, Ariquemes, Brazil

<sup>2</sup>Department of Informatics, Federal University of Maranhão, Brazil

<sup>3</sup>Institute of Computing, Federal Fluminense University, Brazil

Keywords: 3D Breast Models, Thermography Images, Edge Detection.

Abstract: This study enhances the three-dimensional reconstruction of the breast surface from two-dimensional thermal images at five different angles. The process involves the use of a convolutional neural network U-net for image segmentation, extraction of relevant points and curves, geometric transformations to add a dimension to the curves, and modeling with Rational Non-uniform B-splines Surface (NURBS). The work aims to improve the previously proposed algorithm by making modifications to the rotation points and cutting regions to achieve a more comprehensive breast contour. In a quantitative evaluation of the results, comparing thermal images and Structured Light Scanner images with the Costa's and new algorithm, we observed that, concerning scanning, the Costa's algorithm has an average of 37.07% with a standard deviation of 6.27, while the new algorithm exhibits an average of 14.06% with a standard deviation of 7.28. When compared to thermal images, the Costa's algorithm has an average of 37.47% with a standard deviation of 7.24, whereas the new algorithm shows an average of 14.77% with a standard deviation of 7.37. These results indicate that the new algorithm significantly improves the representation of the breast shape compared to the Costa's algorithm.

## 1 INTRODUCTION


Breast cancer is the most common type of cancer among women and the second most death related (Bray et al., 2018). With an early diagnosis and proper treatment in the beginning, it can be curable (Venkataramani et al., 2015; Koay et al., 2004). There are many possible exams to detect a breast cancer, but the mammography is the most popular (Otmami et al., 2024). Besides being an invasive exam, it is considered the gold standard (Koay et al., 2004).


The thermography is a non-invasive exam that analyses the heat distribution over the body (breast region in this case) (Pricigalli et al., 2023). It is accessible, fast, propitiates very early detection due to the possibility of detection of the beginning of the huge cellular multiplication of the cancerous are and its the usage on dense breast for young woman observations (Lanisa et al., 2014; Jockers, 2019). An abnormal heat


distribution on the images can be related to the cancer formation, as long as it can increase the metabolism of the area. But computational tools are necessary to help specialists on decision about whereas there is a benign or malignant nodule in a mamothermography examination (Borchardt, 2013).


The diagnosis of thermography exams is made by analyzing the captured images looking for abnormal features. (Raghavan et al., 2023). Thermography images follows the protocol proposed by (Silva et al., 2014) using static and dynamic data acquisitions. Twenty images are captured after cooling the patient while the person body surface is returning to the environmental temperature (natural warm) in the dynamic data acquisition protocol. Moreover, only five images are taken by using the static protocol.

However, static acquisitions are taken positioning the patient in five different angle in relation to the camera frontal direction position. In order to have a good observation of the breast the angles between the coronal body frontal plane and the camera must be  $0^\circ$ ,  $+45^\circ$ ,  $-45^\circ$ ,  $90^\circ$  and  $-90^\circ$ . These directions form the named frontal view ( $0^\circ$ ), positive and negative oblique views and positive and negative side ( $90^\circ$  and  $-90^\circ$ )

<sup>a</sup> <https://orcid.org/0000-0003-1911-1555>

<sup>b</sup> <https://orcid.org/0009-0006-0429-6074>

<sup>c</sup> <https://orcid.org/0000-0002-3709-8385>

<sup>d</sup> <https://orcid.org/0000-0003-0782-2501>

views.

Each specific direction and view is important to increase the possibility of identification of an breast abnormalities. Side images are as important as frontal images are (Jeyanathan et al., 2018), and an abnormality not seen on frontal image can be seen on a side acquisition. Moreover, they allow not only a best view but the possibility of combine the information from all images captured separately (Silva, 2010).

Mainly when for more complex diagnosis one needs to make correlations among the images. However in such case for combination of all views, its is necessary to have a tools for make easier to have a unique form to visualize all five images captured in one static exam. The aim of this work is to present a methodology developed to unify the 5 views in a 3d model properly. Using this, specialist can begins to analyze the model without the need of mental combination or no longer necessity to correlate the images manually (Costa et al., 2023).

In this paper, we propose a methodology to make a tool that automatic constructs three-dimensional breast models based on the five images from static thermography exams (i.e. images of same patient breasts from different angles). Data used were acquired under a consent of the ethics committee of our university hospital and ministry of health, being publicly registered. To accomplish the objective, it is necessary to make breast segmentations; extract the key points and relevant curves from the images; correlate spatially the key points; correctly positioning and orientation of the curves; increase the dimensional information of the edge points; create a rational smooth surface and include texture mapping to render the synthetic tri dimensional model.

In the next section, a review of related works on breast modeling is explored. After, the approaches used in this study is presented in Section 3, outlining the procedures and techniques used for the three-dimensional modeling of breasts. Section 4 discusses the results, highlighting the contributions and implications of our propositions. Section 5 compares the results, presenting conclusions and suggestions for future research in this scope.

## 2 RELATED WORKS

This section presents some works on 3D modelling of the breast in chronological order.

Silva (2010) developed a three-dimensional reconstruction method for breasts using thermal images in different positions. The algorithm utilizes body contours, curves fitted by least squares, and

the NURBS (Non-Uniform Rational B-Splines) technique to generate 3D meshes. A software was implemented to create three-dimensional models from infrared exams, highlighting variations between the actual body and the generated model. However, the study did not focus on 3D visualization tools for exams (Silva, 2010).

Ciechomski et al. (2012) developed a computational tool for the three-dimensional reconstruction of the breast from digital photos taken also at three angles (frontal, right lateral, and left lateral). The generation of the 3D model is based on the identification of points provided by the user in the 2D images. In this approach some measurements must be manually included, as the distance between the nipples and from the nipple to the infra mammary fold.

As the main goal of Ciechomski et al. (2012) is surgery planning, the physician carries out the planning must define positions and diameters of the implants for simulation. The software facilitates the three-dimensional visualization of the breast outcome. However, it is worth noting that the software requires user intervention (Ciechomski et al., 2012).

Viana (2016) created a 3D representation of the female breast using points from infrared images generated by a computational program. A MATLAB® program corrected coordinates for breast reconstruction, and the resulting wireframe was exported for Computational Fluid Dynamics (CFD) preprocessing. The breast's internal structure was modeled with 3D volumes, replacing lobes, lactiferous ducts, and anomalies from patient examinations. Tools such as Gambit<sup>TM</sup>, DesignModeler®, and Meshing<sup>TM</sup> prepared the geometry for temperature calculations, while Fluent® software calculated temperature values at mesh points (Viana, 2016).

Costa (2020) introduced an innovative algorithm for automated 3D breast model construction, utilizing five images per patient: frontal, oblique right lateral, oblique left lateral, total right lateral, and total left lateral. Automatic segmentation employed the U-net convolutional neural network across all views. Nine curves, six corresponding to main images and three auxiliary, were created considering different angles. These curves were B-spline adjusted, and model surfaces were generated using Non-Uniform Rational B-Splines (NURBS) from the generated points. While the model received majority approval from 15 experts, some noted shortcomings included lack of edge smoothing, decentralized nipple texture, model flattening, and inadequate depth representation in patients with larger breasts (Costa et al., 2023).

Saha (2023) addresses the challenge of visualizing the complete 180° mammary region using only 2D

thermal images, reconstructing 3D thermal images of the breast surface from 2D thermal images captured at different viewing angles (Saha et al., 2023). The method consists of five main steps: foreground segmentation, 3D mammary silhouette generation, 2D visualization generator, loss function, and overlap function. The segmentation process is applied using the Otsu binary segmentation method to each of the five thermal views captured at different angles, resulting in corresponding 2D mammary silhouettes. These silhouettes are utilized in a CNN encoder-decoder architecture to generate the 3D mammary silhouette, which is then employed to obtain random projections of the silhouettes. The loss function minimizes the distance between the generated 2D projections and the actual silhouettes of the input 2D thermal images, and the overlap function maps the input temperature values onto the generated 3D silhouette.

### 3 METHODOLOGY

We here present details of how the three-dimensional breast surface is constructed from five two-dimensional thermographic images obtained at the angles of  $0^\circ$ ,  $45^\circ$ ,  $90^\circ$ ,  $-45^\circ$ , and  $-90^\circ$ . Basically, the reconstruction algorithm addresses five main steps: (1) segmentation of the 5 original 2d images, extraction of relevant 2d points and plane curves (i.e. in the plane of each image), (2) geometric transformations of these 2d to 3d points and plane curves to their 3d orientation and position; (4) increasing the dimensional information of the control points to allow 3d borders, (5) 3d surface modelling by using Rational Non-uniform B-splines Surface (NURBS) for breast representation of volunteers, and its rendering.

This work is dedicated mainly to correct some previous drawn-back of the NURBS construction, it is in step 2. We here suggest a set of modifications in the rotations points and cutting regions to achieve more complete and smooth breast representations.

#### 3.1 Image Acquisition

This work uses a public data from (Silva et al., 2014) and available online at *Visual Lab DMR* website ([visual.ic.uff.br/dmi](http://visual.ic.uff.br/dmi)). The images have a resolution of  $640 \times 640$  pixels, and are achieved with a thermographic camera FLIR® SC620. The acquisition protocol captures 25 images for each patient, 20 are under induced superficial temperature modification (dynamic protocol), and 5 under constant temperatures (static protocol) (Silva et al., 2014). Only the static 5

images are used on this work methodology.

Each image represents a different angle between the camera frontal direction and the patient coronal plane. Frontal view captures the body plane in the same direction of the frontal camera plane, that is the angle between them is  $0^\circ$ . Figure 1 first image shows this view. The oblique on the right lateral view captures the body rotated to  $45^\circ$  to the right around the cranium-caudal body axis: Figure 1 second image shows this view. Oblique on the left lateral view, orientated for acquisition the body rotated around  $45^\circ$  to the left in this axis (Figure 1 fourth image shows this view). The right lateral view puts the body rotated to  $90^\circ$  to the right before acquisition (Figure 1 third image shows this view). The left lateral view rotated to  $90^\circ$  to the left the body as can be observed in the final image of Figure 1).

The proper functioning of the image processing and edge detection algorithm depends on ensuring that the 5 input images meet specifications, being captured without blur or other errors. In lateral images, it is crucial that the contour of the breasts is visible. Examinations revealing anomalies in breast shape are considered only if the visibility of one breast's silhouette is not impaired by the other. A preprocessing step is incorporated to eliminate inputs and preserve the accuracy and reliability of the algorithm's output.

#### 3.2 Preprocessing

Initially, a simple conversion is performed from temperature data stored for the images to the gray scale, which operates with only one channel per image. The conversion is expressed by Equation 1, where, for an image  $P$ ,  $P_{ij}$  represents the temperature value of a point  $(i, j)$  of the stored image array. The minimum and maximum temperatures in a matrix are denoted by  $min$  and  $max$ , respectively. The result,  $m_{ij}$ , corresponds to the new gray scale value of each pixel, allowing good contrast and visibility of the temperatures:

$$m_{ij} = 255 \times \frac{P_{ij} - \min}{\max - \min} \quad (1)$$

In the preprocessing step, the dimension of the gray scale images is also transformed from  $640 \times 480$  to  $256 \times 256$ . These new images will be used in the automatic segmentation process.

The frontal view images of the exams will be used exclusively for the texture mapping in the rendering step of the three-dimensional model. To obtain a color representation of this view, their pixels are converted from gray scale to the RGB (Red, Green, Blue) color system, following the Look Up Table (LUT) of the FLIR Rain palette color levels.

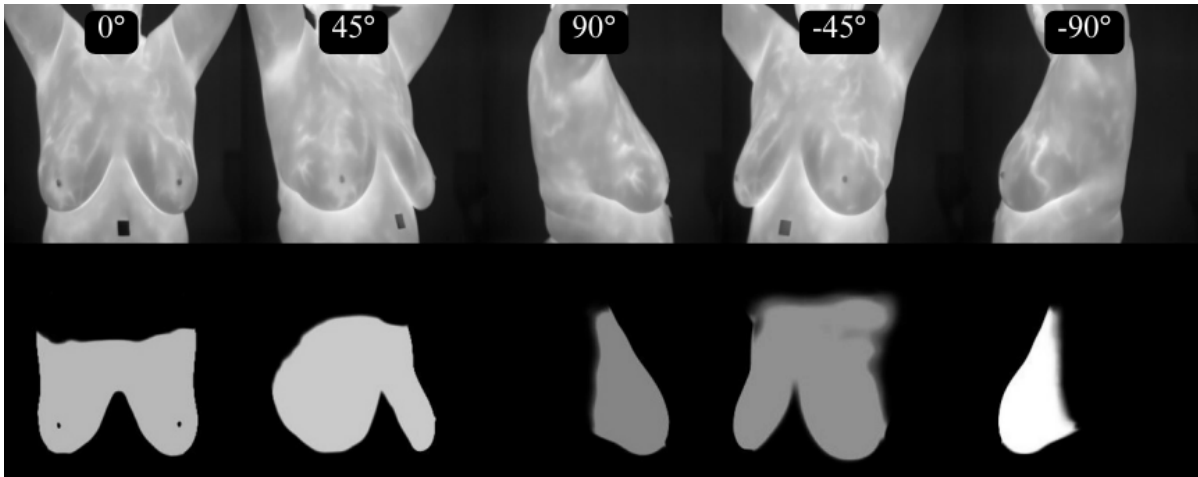


Figure 1: Five images of an thermography exam with the body and camera at five positions. Frontal ( $0^\circ$ ), oblique on the right lateral ( $45^\circ$ ), right lateral ( $90^\circ$ ), oblique on the left ( $-45^\circ$ ) and left lateral ( $-90^\circ$ ) (first line). Example of automatic segmentation output using a U-Net architecture and the learned hyper-parameters (second line).

### 3.3 2D Border Segmentation

The segmentation of the region of interest (ROI) of the breasts is performed using a deep learning technique, specifically the architecture of a Convolutional Neural Network (CNN) named U-Net (Ronneberger et al., 2015) (Dalmia et al., 2018).

Considering all the data set of patients, a subset used, 109 (78%) exams were used for training the nets and 31 (22%) were separated from the database for testing. The training used 100 epochs in batches of 2 with 50 epochs. Net weights are initialized with normal distribution of random values. Each convolution uses the rectified linear unit activator (*ReLU*) function to allow passing values that are greater than zero (0). Adam optimizer with learning rate  $1 \times 10^{-4}$  is used (zhixuhao, 2023). This allows the region of the breasts to be separated (i.e. segmented) from the rest of the image, as shown in Figure 1. In this figure the first line of images represents the gray scale input to the U-net and the second line the segmented results.

After segmentation with the U-net, it is necessary to perform a filtering step to remove unnecessary areas. This is achieved by applying a grayscale threshold using the Suzuki approach, transforming the image into binary (Suzuki et al., 1985). Subsequently, only the area with the highest number of pixels in each direction is retained. The Canny edge detection method is then applied to obtain only the largest connected edges in each direction. This process is detailed in (Costa et al., 2023).

### 3.4 Relevant Edge

Identifying relevant edges and points in each view (Figure 2) is crucial for understanding breast shape in width (front views) and depth, thickness, and height (lateral obliques and side views). These elements are later used to generate 3D information, transforming plane curves into spatial ones for surface modeling.

The infra-mammary curve holds particular importance in this process and serves as a reference to position other curves. Through the identification of relevant edges and points in each view, a unified 3D coordinate system is established. The four-step process is employed to identify these relevant edges.

Initially, the algorithm locates points in the lower region of each edge by searching for the first pixels from bottom to top in the output of the previous step. This ensures that only the pixels closest to the bottom of each of the five edges are stored. Then, a vertical search is conducted, starting from the right side of each image. Unlike the bottom search, the lateral search involves scanning each final edge pixel from the right end to find the closest pixels on this side. The same approach is applied to define the left edge, finding the closest pixels on this side.

In the final step, pixels from the first step that are found three times in steps 2 and 3 are removed. This ensures the exclusion of points present in the relevant edges on the right and left sides. The resulting points constitute the basis for subsequent 3D modeling. This process is detailed in (Costa et al., 2023).



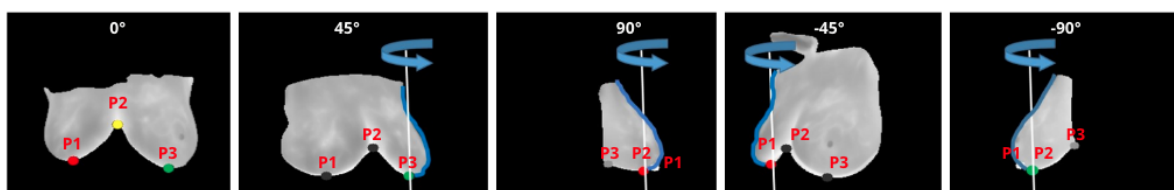


Figure 2: Identification of the relevant edges and key points of each direction.

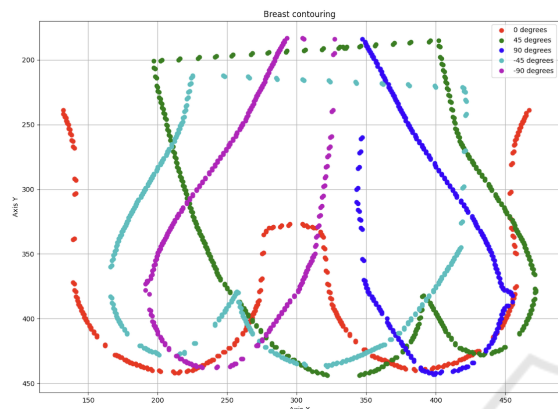


Figure 3: Relevant edges in a two-dimensional plane: Red color represents the points from the frontal view; the two tones of Green color represent the points from the oblique views; magenta and blue colors represent the points from the side view.

### 3.5 Key Points of Breast Edges

Extraction of each view relevant breast edges points for each examination angle (or for each view) must be done. For each 2d curve of the last step, this process consists of the identification of three points named P1, P2 and P3. Figure 2 shows these points in the images resulting from segmentation of relevant edges in order to better identify their meanings. These points belong to the lower single edge of the 5 views, that is, from final step of the previous subsection.

On the  $0^\circ$ ,  $45^\circ$  and  $-45^\circ$  images, a point is found at the junction of the infra-mammary curves, in the center of the body, this is named P2, Other two points correspond to the inflections of the infra-mammary curves on the right (named P1) and left (P3). For side images of  $90^\circ$  and  $-90^\circ$ , the beginning and end of the curve are identified, they are named P1 and P3, and presented on Figure 2(d). For these view, a third point (named P2) is defined by lowest point of these curves.

### 3.6 Geometric Transformation and 3D Representations

After segmenting the breast limits in various directions in the 2D plane, key points identified in the pre-

vious step play a crucial role in translating and rotating the 2D curves to their correct positions in a three-dimensional space.

A 3D coordinate system is employed, where the X and Y axes align with the 2D image's horizontal and vertical directions, respectively, and the Z-axis is determined by the cross product of X and Y. The translation of curves involves moving them to the identified key points, and subsequent rotation is based on the view directions, creating a 3D representation for surface generation.

Curves, such as those from  $45^\circ$  and  $-90^\circ$  views, undergo rotation by their respective angles. For instance, curves from  $45^\circ$  and  $90^\circ$  views are translated to point P3, while curves from  $-45^\circ$  and  $-90^\circ$  views are moved to point P1 on the frontal contour (see Figure 4). This results in rotated curves with diverse 3D coordinates based on their rotation angles. To enhance the 3D representation, auxiliary contours are created by replicating contours from  $45^\circ$  and  $-45^\circ$  views to new positions, forming curves rotated by  $135^\circ$  and  $-135^\circ$  (which rotate at around P3 and P1, respectively). These contribute to the formation of an internal curve resembling a valley between two mountains relief. Figure 4 displays these curves. After this step, the algorithm eliminates all points located above the zero point on the Z axis, revealing only the surface of the breast (see Figure 5).

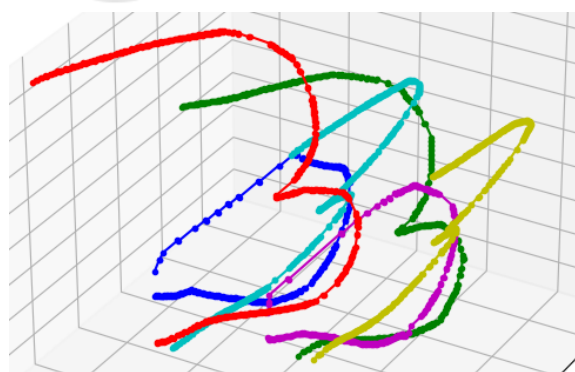


Figure 4: The main curves after their translation and rotation and the auxiliary curves at  $135^\circ$  and  $-135^\circ$ , in yellow and red, included for modeling the surface of the breast regions.

### 3.7 Surface Modelling

So far, six curves that play a crucial role in determining the breast shape have been identified. In addition to these, three more curves are incorporated to compose the model, representing the lateral and central profile of the body. These curves are derived from the  $0^\circ$  image, with the first capturing the left contours, the second capturing the right contours, and the central curve generated by connecting the P1 points to a straight line to the top of the image. This process results in a total of nine curves: (1) right frontal curve, (2) left oblique lateral curve, (3) total lateral (right  $90^\circ$  angle) curve, (4) left oblique auxiliary curve, (5) central auxiliary curve, (6) right oblique auxiliary curve, (7) total lateral (left  $90^\circ$  angle) curve, (8) right oblique curve, (9) left frontal curve. Figure 5 shows all these curves.

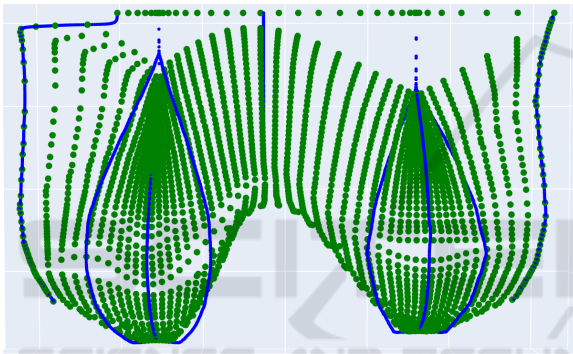


Figure 5: The set triangular mesh limit points of generated curves parallel to the cranium caudal body direction used for rendering the final surface.

These nine 3D curves are initially described by all their points (raster format). However, for better description and surface generations, they must be transformed into vector form, i.e., through mathematical expressions.

As the number of points on each of these curves is different, an adjustment is used before these. They are normalized to represent the same number of control points for each curve. The B-spline function implemented in (Bingol and Krishnamurthy, 2019) is employed for this purpose.

The nine (9) B-Splines curves (in blue) and NURBS Surface created are shown in Figure 5 by green dots. They represent the vertices of the triangles that generated the mesh, obtained after applying a generator of the surface by NURBS (Azevedo and Conci, 2003) and delete all positive points (Costa et al., 2023). The final red shaded surface of these process can be observed in Figure 6.

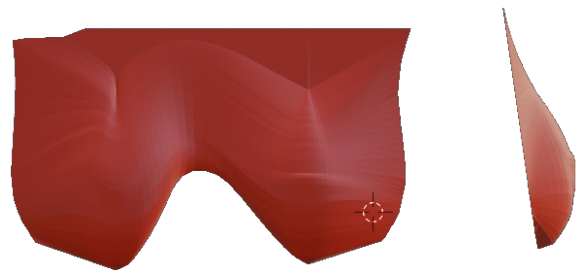


Figure 6: Output of Costa's algorithm showing smaller breast volume than the patient's breast.

## 4 SURFACE IMPROVEMENTS

For the surface, only the curves representing the breast shape are necessary. For this reason, Costa's original algorithm discards points that have positive Z-axis coordinates (Costa et al., 2023). The result is a surface that does not fully represent the breast shape on  $90^\circ$  lateral views and includes some irregular appearing like folders, protrusions and superficial pleats in the upper parts.

In the quest to refine the model, the decision was made to display the complete curvature of the breast in the  $90^\circ$  images. The new approach involves excluding points with Z coordinates greater than the Z coordinate of P3 (representing the end of the infra mammary region and being the point closest to the body's center, as shown in the Figure 2). Due to variability in the position of these points, a strategy was adopted to calculate the Z average between the two P3 points from the  $90^\circ$  and  $-90^\circ$  curves (referred to as PM3). This has the effect of slightly shifting the curve end to include some ascendant curve points, providing a more accurate representation of breast anatomy.



Figure 7: New algorithm result: the complete shape of the side of the breast is represented.

Another modification to the previous model is made by translating all Z points of the right frontal curve and the left frontal curve to PM3, that is responsible for defining the trunk shape. This change ensures a more rounded profile for the body. Figure 7 show the result achieved with this modification. Com-

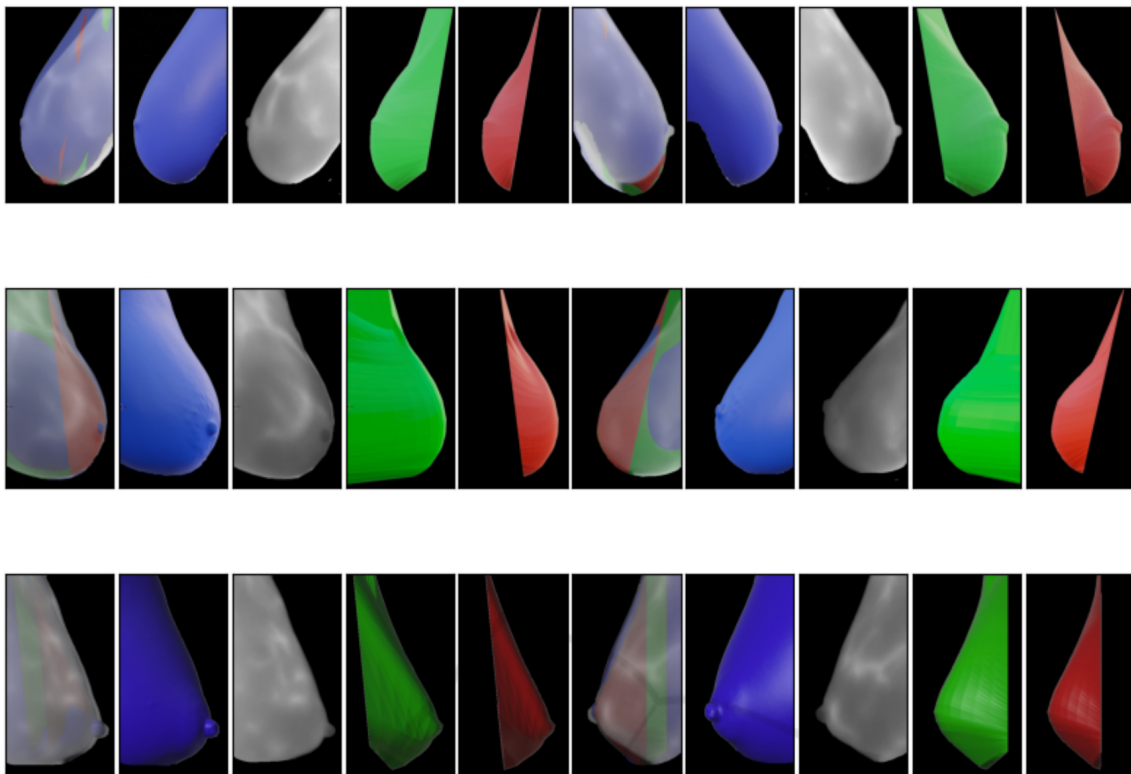


Figure 8: Blue: Structured Light Scanner; Gray: FLIR camera; Green: New algorithm; Red: Costa's algorithm.

paring the lateral breast contours of both results (i.e Figure 7 and Figure 6), it is possible to see that now the resulting surface is more realistic.

site (<https://sites.google.com/view/three-dimensional-breast-model>).

## 5 COMPARING RESULTS

In the present study, a qualitative and quantitative comparison was carried out between the surfaces created by Costa's algorithms and the new algorithms, as well as 3D images acquired using the structured light scanner and 2D images captured by the FLIR camera at angles of  $90^\circ$  and  $-90^\circ$  degrees, through image analysis, using data from 3 volunteers. The objective was to contrast the models generated by the previous algorithm with those produced by the new algorithm, as well as to analyze the Symmetric Difference between the data coming from the structured light scanner scan and FLIR (Conci and Kubrusly, 2017).

Using Blender® software, all 3D models and 2D images were superimposed respecting the same limits, see figure 8. The proposed image comparison algorithm uses a visual approach, binarizing each image of interest and then calculating the symmetric difference between each corresponding pixel in the two models, see the example in the figure 9. More images available online on the web-



Figure 9: Binarized images of the New model (left) and Structured Light Scanner reconstruction (center) of volunteer 1 at 90 degree angle. In the last image on the right, the symmetric differences between the two images is displayed in white.

Table 1 displays the percentage of difference between each volunteer's models for the 90 and -90 degree angles. These values allow comparisons between thermal images (FLIR) and Scanner acquisitions (Scan) with the Costa's algorithm (Old) and new algorithm (New). This table shows, in the bottom line, the Standard Deviation (SD) of the 6 views used: the biggest difference in the average values (line 8) is in

Table 1: Between breast relative symmetric differences, means and standard deviations (SD).

Volunteer-angle	New/Old	Scan/Old	Flir/Old	Scan/New	Flir/New	Flir/Scan
1-(-90°)	20.75%	34.90%	38.66%	16.39%	19.45%	4,63%
1-(90°)	19.92%	39.79%	37.43%	20.30%	18.87%	5,74%
2-(-90°)	28.41%	29.67%	27.86%	4.39%	6.10%	5.34%
2-(90°)	47.50%	47.97%	49.75%	5.58%	5.19%	2.96%
3-(-90°)	17.36%	33.86%	33.31%	16.74%	16.23%	1,91%
3-(90°)	18.31%	36.21%	37.82%	20.97%	22.78%	3.26%
<b>Mean</b>	25.38%	37.07%	37.47%	14.06%	14.77%	3.97%
<b>SD</b>	11.52	6.27	7.24	7.28	7.37	1.50

the Scan/Old and Flir/Old columns. Considering the DP (line 9), the most critical variation occurs between the New and Costa's algorithm.

## 6 CONCLUSIONS

We can see that the new model represents the breast with a more pronounced lateral contour, more faithfully reflecting the anatomy of the body. The comparison between the previous model and the new model highlights that there were no significant changes in the shape of the model's surface, but rather in the total volume of the surface included in the breast.

In a quantitative evaluation of the results, comparing FLIR acquisitions (thermal images) and Scanner with the Costa's algorithm and New algorithm, we observed that, concerning scanning, the Costa's algorithm has an average of 37.07% with a standard deviation of 6.27, while the New algorithm exhibits an average of 14.06% with a standard deviation of 7.28. When compared to thermal images, the Costa's algorithm has an average of 37.47% with a standard deviation of 7.24, whereas the New algorithm shows an average of 14.77% with a standard deviation of 7.37 (see Table 1). These results indicate that the New algorithm significantly improves the representation of the breast shape compared to the Costa's algorithm.

However, improvements are still possible in the frontal representation, as well as in adjusting the alignment of the curves in the upper region of each breast.

It is important to highlight that textures were not incorporated in this work. Therefore, this is the objective of future research, which is the development of merging all five images into a single textured 3D object, enabling an overview of infrared scans.

## ACKNOWLEDGEMENTS

E.L.S.M. is supported by Federal Institute of Education, Science and Technology of Rondônia (IFRO). A.C. is supported in part by the National Institutes of Science and Technology (INCT - MACC project), National Council for Scientific and Technological (CNPq) under grant 307638/2022-79, the Research Support Foundation of Rio de Janeiro State (FAPERJ) over CNE, e-Health Rio and Digit3D ("temáticos") projects (Digit3D projects, 2023).

## REFERENCES

- Azevedo, E. and Conci, A. (2003). *Computação gráfica: teoria e prática*. Elsevier, Rio de Janeiro.
- Bingol, O. R. and Krishnamurthy, A. (2019). NURBS-Python: An open-source object-oriented NURBS modeling framework in Python. *SoftwareX*, 9:85–94.
- Borchardt, T. (2013). *Análise de imagens termográficas para a classificação de alterações na mama [Analysis of thermographic images to classify changes in the breast]*. PhD thesis, Instituto de Computação, Universidade Federal Fluminense, Niterói, RJ, Brasil.
- Bray, F., Ferlay, J., Soerjomataram, I., Siegel, R. L., Torre, L. A., and Jemal, A. (2018). Global cancer statistics 2018: Globocan estimates of incidence and mortality worldwide for 36 cancers in 185 countries. *CA: a cancer journal for clinicians*, 68(6):394–424.
- Ciechomski, P. H., Constantinescu, M., Garcia, J., Olariu, R., Dindoyal, I., Huu, S. L., and Reyes, M. (2012). Development and implementation of a web-enabled 3d consultation tool for breast augmentation surgery based on 3d-image reconstruction of 2d pictures. *Journal of Medical Internet Research*, 14(1):e21.
- Conci, A. and Kubrusly, C. (2017). Distance between sets - a survey. *Advances in Mathematical Sciences and Applications*, 26(1):1–18.
- Costa, G., Moura, E., Borchardt, T., and Conci, A. (2023). Modeling the 3d breast surface using thermography. In Kakileti, S., Manjunath, G., Schwartz, R., and Frangi, A., editors, *Artificial Intelligence Over Infrared Images for Medical Applications (AIIMA*



- 2023), volume 14298 of *Lecture Notes in Computer Science*, page 45–56. Springer.
- Dalmia, A., Kakileti, S. T., and Manjunath, G. (2018). Exploring deep learning networks for tumour segmentation in infrared images. In *14th Quantitative Infrared Thermography Conference*, Berlin, Germany. DGZfP.
- Digit3D projects (2023). Digit3d projects. Acessado em 8 de novembro de 2023.
- Jeyanathan, J. S., Shenbagavalli, A., Venkatraman, B., and Menaka, M. (2018). Analysis of breast thermograms in lateral views using texture features. In *TENCON 2018 - 2018 IEEE Region 10 Conference*, pages 2017–2022, Jeju Island, Korea.
- Jockers, D. (2019). Thermography: The new gold standard in breast cancer screening.
- Koay, J., Herry, C., and Frize, M. (2004). Analysis of breast thermography with an artificial neural network. In *The 26th Annual International Conference of the IEEE Engineering in Medicine and Biology Society*, volume 1, pages 1159–1162, San Francisco, California. IEEE.
- Lanisa, N., Cheok, N. S., and Wee, L. K. (2014). Color morphology and segmentation of the breast thermography image. In *2014 IEEE Conference on Biomedical Engineering and Sciences (IECBES)*, pages 772–775, Miri, Sarawak, Malaysia. IEEE.
- Otmani, I., Amroune, M., Rahmani, F. L., Soltani, H., Benkhelifa, E., and Conci, A. (2024). Lamis-dmdb: A new full field digital mammography database for breast cancer ai-cad researches. *Biomedical Signal Processing and Control*, 90:105823.
- Pricigalli, N., Moura, E., and Conci, A. (2023). Is symmetry important in breast infrared examinations? In Kakileti, S., Manjunath, G., Schwartz, R., and Frangi, A., editors, *Artificial Intelligence Over Infrared Images for Medical Applications (AIIIMA 2023)*, volume 14298 of *Lecture Notes in Computer Science*, page 67–79. Springer.
- Raghavan, K., B, S., and v, K. (2023). Attention guided grad-cam: an improved explainable artificial intelligence model for infrared breast cancer detection. *Multimed Tools Appl.*
- Ronneberger, O., Fischer, P., and Brox, T. (2015). U-net: Convolutional networks for biomedical image segmentation. In *International Conference on Medical image computing and computer-assisted intervention*, pages 234–241, Heidelberg, Berlin. Springer.
- Saha, A., Kakileti, S., Dedhiya, R., and Manjunath, G. (2023). 3d-breastnet: A self-supervised deep learning network for reconstruction of 3d breast surface from 2d thermal images. In Kakileti, S., Manjunath, G., Schwartz, R., and Frangi, A., editors, *Artificial Intelligence Over Infrared Images for Medical Applications (AIIIMA 2023)*, volume 14298 of *Lecture Notes in Computer Science*. Springer, Cham.
- Silva, L., C. M. Saade, D., Sequeiros Olivera, G., Silva, A., Paiva, A., Bravo, R., and Conci, A. (2014). A new database for breast research with infrared image. *Journal of Medical Imaging and Health Informatics*, 4(1):92–100.
- Silva, S. V. (2010). *Reconstrução da Geometria da Mama a partir de Imagens Termográficas [Reconstruction of Breast Geometry from Thermographic Images]*. PhD thesis, Computer Institute. Universidade Federal Fluminense, Niteroi, Brazil.
- Suzuki, S. et al. (1985). Topological structural analysis of digitized binary images by border following. *Computer vision, graphics, and image processing*, 30(1):32–46.
- Venkataramani, K., Mestha, L. K., Ramachandra, L., Prasad, S., Kumar, V., and Raja, P. J. (2015). Semi-automated breast cancer tumor detection with thermographic video imaging. In *2015 37th Annual International Conference of the IEEE Engineering in Medicine and Biology Society (EMBC)*, pages 2022–2025, Milan, Italy. IEEE.
- Viana, M. (2016). *Reconstrução tridimensional da mama feminina a partir de imagens médicas por infravermelho com auxílio de geometrias substitutas [Three-dimensional reconstruction of the female mother from infrared medical images with the aid of surrogate geometries]*. PhD thesis, Universidade Federal de Pernambuco.
- zhixuhao (2023). Github - zhixuhao/unet. Acessado em 8 de novembro de 2023.